Equivalent geometrical imperfections for local and global interaction buckling of welded square box section columns

M. Radwan [*], B. Kövesdi

Budapest University of Technology and Economics, Faculty of Civil Engineering, Department of Structural Engineering, Műegyetem rkp. 3., 1111 Budapest, Hungary

ABSTRACT

The demand for welded box-sections is increasing in the construction industry due to their easy fabrication and limited stability issues compared to other open sections. The instabilities of welded box-section can be mainly categorized into three types: global buckling, local buckling, and interaction buckling. Nowadays, more attention is paid to interaction buckling, as designers tend to use lighter sections to save on weight and cost. Nevertheless, there is no suitable method to consider the nonlinear effect of interaction between the global and the local buckling, which can be directly incorporated using FEM-based design. Moreover, the currently adopted equivalent geometrical imperfections for flexural buckling in the Eurocode were developed based on geometric nonlinear imperfect analysis (GNIA), and it is inappropriate to be used in geometrically and materially nonlinear analysis (GMNIA). Therefore, the current research investigates the accurate application of the imperfections and imperfection combinations for welded box-sections using the GMNIA technique to determine the accurate buckling resistance by the FEM-based design approach. The investigation starts with developing a numerical model and validating it against test results available in the literature. The validated numerical model is used to conduct a parametric study to find the accurate buckling resistance using previously developed combinations of geometrical imperfections and residual stresses. Then, additional parametric studies are executed to back-calculate the necessary equivalent global and local imperfections and find a suitable rule for combining the global and local imperfections based on the accurate buckling resistance. The proposed equivalent geometric imperfection magnitudes can be applied in the numerical model to aid in the FEM-based design approach.

1. Introduction

Welded box-sections have limited structural instabilities compared to the other sections available for the construction industry. Mainly, three types of instabilities can be identified, including global, local, and interaction buckling. Globally and locally slender sections are susceptible to interaction buckling instability, where the section will experience a combination of large global and local deformations. Different researchers investigated the interaction buckling of welded box sections emphasizing that the currently available methods in the Eurocode [1] do not take into account the nonlinear interaction between the global and the local buckling behaviour. Therefore, the current study aims to investigate the interaction buckling resistance of welded box-section columns, taking into account the nonlinear effect of interaction and using the obtained accurate resistance to back-calculate global and local equivalent geometrical imperfections that can be used in FEM-based design.

In general, design for buckling can be done either by using buckling curves available in the Eurocode using specific checks for global and local buckling or by utilizing FEM-based design approaches if the numerical model can capture the buckling phenomena correctly. Geometrical and material nonlinear analysis (GMNIA) using imperfections is a second-order analysis that is able to capture such buckling behaviour leading to a more accurate estimation of the buckling resistance and better distribution of forces and stresses if suitable imperfections and residual stresses are modelled. In practice, modelling residual stresses can be challenging; therefore, equivalent geometrical imperfections for GMNI analysis-based resistance calculation are developed to take into account the effect of residual stresses and geometric imperfections in a combined way.

A limited number of researchers investigated the interaction buckling resistance of welded box-section columns. Schillo et al. [2] investigated high-strength steel welded box sections. The authors developed a new design method that utilises the same procedures as given in the

EN1993-1–1 with a new equivalent geometrical imperfection factor that considers the loss of stiffness due to local buckling instead of using the effective width method. The authors found that the results of the Eurocode are significantly scattered compared to their results. Degée et al. [3] performed a parametric study and an experimental test program to study the interaction buckling. The authors developed a modified global slenderness ratio calculation method $\overline{\lambda}_{int}$ that includes a modifying factor β using the ratio of the gross cross-sectional moment of inertia (I) and the effective moment of inertia (I_{eff}) to consider the loss of flexural stiffness. Also, the local buckling reduction factor ρ was used to account for the loss of stiffness due to local buckling. These factors are applied to the global slenderness ratio $\overline{\lambda}_g$ to account for the interaction buckling. An upgrade from the Eurocode curve "b" to curve "a" was suggested as it was found that the buckling resistance of class 4 welded box section column is higher than the currently adopted by the Eurocode. Both previously mentioned researchers suggested a further investigation.

Numerous researchers criticized the application of the Winter-type buckling curve that is given in the EN1993-1–5 [4], as it overestimates the local buckling resistance of welded box-sections [5]–[7]. The currently adopted local equivalent geometrical imperfections available in Table C.2 of EN1993-1–5 [4] utilises a local imperfection of $b/200$ for panels or subpanels. This imperfection amplitude was mainly calibrated to the Winter-type buckling curve and yielded local buckling resistances conforming to it. Therefore, a new calibration was performed by the authors in previous research to estimate the buckling resistance according to the buckling curve available in Annex B of the Eurocode EN1993-1–5 [4]. Furthermore, the authors developed equivalent geometrical imperfections calibrated against the buckling curve developed by Schillo and Feldmann [8]. This buckling curve was proven highly reliable based on test results and advanced numerical simulation results [6]. Many researchers considered $L/1000$ as a suitable global imperfection to be used in numerical models to study the global buckling if residual stresses are also applied [2]. Therefore, in the current paper, the previously developed, reliable geometrical imperfections and well-established residual stress models are applied to determine the accurate interaction buckling resistance. The numerical model is validated against available experimental test results taken from the literature. Then the numerical model is used to perform a large parametric study on a wide range of global and local slenderness and for three steel grades between S235 and S460 to find suitable local and global equivalent geometrical imperfections and their combinations. The equivalent geometrical imperfections will be found by calibrating the numerical model against the accurate interaction resistance calculated using residual stresses and geometric imperfections in the numerical model. The current investigation has two results: (i) at first, it determines the accurate imperfections combination rules depending on the local and global slenderness ratios leading to accurate interaction buckling resistance, (ii) evaluates different imperfection combination rules choosing one leading and one accompanying imperfection and determine their reliability.

2. Literature review

2.1. Previous research results on interaction buckling resistance

Degée et al. [3] studied the interaction buckling behaviour of S355 welded rectangular section columns (RHS). Six samples were tested in this study with global slenderness of 0.35, 0.55, and 0.75 for the same local slenderness of 0.9. A numerical parametric study was carried out for the global slenderness $\overline{\lambda}_g$ of 0.8 to 1.4 and local slenderness $\overline{\lambda}_p$ of 0.7 to 1.1 on rectangular box sections. The authors suggested a global imperfection of $L/1000$ and a local imperfection of $b/1000$ if the residual stresses are applied. Otherwise, $L/750$ as a global imperfection and $b/250$ as local imperfection. The authors found that the buckling curve "b"

was too conservative. Therefore, they suggested an upgrade to the buckling curve "a" for welded box sections. A new method was proposed for normal and high-strength steel based on a new definition of global slenderness to account for the loss of stiffness due to local buckling, and it is called $\overline{\lambda}_{int}$, and it is based on the Eurocode β factor by taking into account the gross to the effective moment of inertia ($\frac{I}{I_{eff}}$) and effective to gross cross sectional area ($\frac{A_{eff}}{A}$), with the adoption of the local buckling reduction factor ρ, leading to a higher resistance as the interaction slenderness $\overline{\lambda}_{int}$ is smaller than the global slenderness $\overline{\lambda}_g$.

Khan et al. [9] studied the structural behaviour and buckling resistance of slender welded box-section columns made of HSS (690 MPa). Fifteen test specimens are examined, and buckling resistances are compared to various international standards, including the Eurocode, AISC, and Australian Standard. The authors investigate the effects of residual stresses on the member capacity using heavy and light welds. The authors carried out a numerical study in which $L/1000$ was used as global imperfection and $b/1000$ as local imperfection with residual stress. Based on the experimental and numerical results, it was found that intermediate-length specimens failed due to the global and local buckling together. Accordingly, the authors suggested utilising a reduction factor that accounts for the combined buckling effect. It was found that all normalised values of the experimental and numerical tests were lying above the buckling curve "b" of the Eurocode and suggested utilising this curve as a suitable curve for determining the interaction buckling. It was also found that there was no significant difference between specimens with heavily and lightly welded sections.

Yang et al.[10] investigated numerically and experimentally on twelve steel columns with medium lengths, the interaction buckling behaviour of welded box-section columns. Two specimens were welded square hollow sections (SHS) and ten with welded rectangular hollow sections (RHS). Test specimens were made of S235 and S355. All specimens under this experimental program failed due to the interaction buckling between the local and the global buckling modes. The authors found that the current specifications are not taking into account the post-buckling capacity of the steel plates, estimating a lower buckling resistance. A numerical parametric study on normal and high-strength steel sections was performed. It was concluded that the buckling curve "a' of Eurocode should be used for steel grades of S960. Also, it was mentioned that the initial imperfections mainly affect the high slenderness sections with an influence of up to 10 %.

Two experiments on S460 and S690 box-section steel columns were conducted by Usami and Fukumoto to investigate the interactive buckling behaviour of high-strength steel columns. An experimental study [11] is carried out on the local and overall interaction buckling behaviour of welded built-up box columns made of high-strength steel. Twenty-seven box-section columns with large slenderness were tested, twenty-four were loaded concentrically, and the rest were loaded eccentrically. Using the test results, an empirical design formula was presented to estimate the interaction buckling strength. Another experimental program [12] was executed by the same authors on a total of twenty-five columns with different lengths and width-to-thickness ratios. Both square and rectangular box sections were tested. A computer program was developed that uses the effective width method to investigate the collapse and characteristics of beam-columns that are suspectable to local buckling. The authors found out that there is a good agreement between the results of the theoretical based computer program and the experimental test results for columns with large width-to-thickness ratio.

Chiew et al. [13] performed 17 tests on eccentric and concentric welded thin-walled box section steel columns made of S235 steel grade leading to various failure modes, including local, overall and interaction buckling. The authors found that the behaviour of long columns with a low width-to-thickness ratio was mainly dominated by overall buckling, while sections with a high width-to-thickness ratio failed due to the combined effect of local and overall buckling, i.e., interaction buckling.

The authors developed an iterative theoretical method to obtain the load and global slenderness curves for various columns under various load conditions using an elastic-perfectly plastic stress–strain diagram to evaluate the stresses and the iterative load based on the curvature, neutral axis, and the total strain of each element. As a result, a set of curves can be obtained for moment-slenderness (M-λ) and load-slenderness (P-λ) and moment-load ($M{-}P$) interaction curves.

Kwon et al. [14] conducted a series of compression tests on welded rectangular hollow section (RHS) columns made of steel material with a nominal yield strength of 315 MPa to study the nonlinear interaction effect experimentally and theoretically. In this method, the authors tried to extend the applicability of the direct strength method (DSM) to welded box-section columns. The DSM method incorporates empirical formulas and elastic buckling stress obtained by buckling analysis and uses a non-reduced cross-section area instead of the effective areas. The proposed formula considers the interaction between the global and local buckling modes as the authors have already investigated the interaction buckling of H-sections. A similar formula was adopted for box-sections with a small reduction because the plates of H-sections have a higher post-buckling reserve.

Schillo et al. [2] performed thirteen tests on square welded box-section columns with a high b/t ratio and made of S500 and S960 steel grades having different global slenderness. The validated numerical model was used to perform a parametric study to determine the reduction factors to design box-section columns experiencing the interaction of both global and local buckling. In this approach, the authors utilised an additional equivalent local imperfection (ep) in the global buckling formula to account for the loss of stiffness due to local buckling instead of using the Eurocode approach, which is the effective cross-sectional method. The proposed value for the equivalent local imperfection is calculated according to Eq. (1). The authors mentioned that the proposed approach is more conservative across the analysed slenderness range and more distinct for eccentrically loaded columns, where the bending is important. Although this approach was developed for high-strength steel structures, it is still a good alternative to compare with, as it utilises the currently adopted Eurocode formula based on the Ayrton-Perry-type formulation of the global buckling resistance; It was validated against test results.

$$ep = s\left[\left(\frac{1}{\chi_A} - 1\right) + \frac{1 - \psi}{1 + \psi}\left(\frac{1}{\chi_W} - 1\right)\right] \tag{1}$$

Where (s) is equal to the moment of inertia (I) divided by the area of the section (A) multiplied by the distance from the neutral axis to the maximum fibre (z) $s = \frac{I}{A.z}$. The parameters χ_A and χ_W are factors calculated using the effective width method $\chi_A = \frac{Aeff}{A}, \chi_W = \frac{W_{eff}}{W}$, ψ is a factor that depends on the eccentricity of the load. In this current research program, only pure compression is studied; therefore, $\psi = 1$ is assigned.

2.2. Previous investigation of imperfection scaling factor

2.2.1. Member buckling imperfection scaling factors.

Global imperfection or bow imperfection is a bow deformation of a stiffener or the entire member. The maximum allowed bow imperfection is currently $L/750$ according to EN 1090–2:2008 + A1:2011[15] (this version has been superseded by EN 1090–2: 2018[16]). Different studies suggested using $L/1000$ as a global imperfection if the residual stresses are modelled[3,17], corresponding to 75 % of the maximum allowed imperfection. Sometimes it is challenging to model the residual stresses; therefore, equivalent geometrical imperfection can be utilised to account for the effect of residual stresses, making the modelling process easier in the FEM-based design approach. Rondal and Maquoi [18] introduced the concept of equivalent bow imperfections, which are adopted in the current buckling curves of the Eurocode and corresponds to sinusoidal initial imperfection. The amplitude of the imperfection is found according to Eq. (2) which is based on the Perry-Robertson

formula, where α (is an imperfection factor defining a particular buckling curve, which is based on a large number of tests, A is the cross-sectional area, and W is the elastic section modulus and $\overline{\lambda}$ is the global slenderness according to Eq. (2)[19].

$$e_0 = \alpha(\overline{\lambda} - 0.2)\frac{W}{A} \tag{2}$$

Lindner et al.[20] investigated the determination of the equivalent imperfection for centrally loaded columns. A sine curve initial bow was adopted and e_0 was assumed to be the maximum amplitude. The equivalent imperfections are calculated by introducing the moment M in an appropriate interaction formula and calculated by the second-order elastic theory, taking into account the initial bow imperfections. That leads to the formula in Eq.(3). where $\psi = 1 - \chi$ for linear plastic interaction. It was assumed that a cross-sectional analysis based on the second-order theory would result in the same load-carrying capacity of the buckling curves in the Eurocode EN1993-1–1.

$$e_0 = \frac{\psi\left(1 - \chi\overline{\lambda}^2\right)}{\chi}.\frac{M_{pl}}{N_{pl}} \tag{3}$$

Lindner et al.[21] suggested tabulated equivalent geometrical imperfections, which are calculated according to Eq.(4), where α is the imperfection factor depending on the buckling curve and accounts for the effect of residual stresses, β is the reference relative bow imperfection, L is the length of the member, ε calculated according to Eq.(4) and accounts for the strength of the material.

$$\frac{e_0}{L} = \frac{\alpha\beta}{\varepsilon} \tag{4}$$

Walport et al.[22] investigated cold-formed steel columns and found that the currently available equivalent bow imperfections that are available in the Eurocode EN1993-1–1 were developed on an elastic basis, and it is not generally appropriate to use these imperfections for nonelastic analysis and imperfection of $e_0 = \frac{\alpha L}{150}$ (α is the imperfection factor set in EC3) was suggested to be used in the GMNIA analysis by calibrating the appropriate imperfections for inelastic analysis based on the GMNIA parametric study, where a global geometrical imperfection of $L/1000$ and residual stresses were used. This equivalent imperfection can be used in the eigenmode method of defining the imperfection or the hand-defined method by modifying the nodes' coordinates.

Jönsson and Stan [17] have analysed I-section columns using the GMNIA technique. It was found that the equivalent geometrical imperfections that correspond to the European buckling curves are inconsistent with the equivalent geometrical imperfections to be used in finite element modelling. The equivalent geometrical imperfections available in the Eurocode result in considerably lower curves. The authors suggested a slight modification to take the influence of yield strength on the buckling curves into account, making the equivalent imperfections independent of the yield strength as presented in Eq. (5), in which the buckling curves of the Eurocode will change depending on the yield strength. In ENV 1993–1–1:1992, slightly smaller equivalent imperfection factors for plastic capacity were suggested compared to the current EN1993-1–1.

$$e = \alpha(\lambda\varepsilon - 0.2)\frac{W}{A} \tag{5}$$

Somodi et al.[23] performed a numerical study on welded box section columns subjected to pure compression to determine equivalent global geometrical imperfections calibrated to the buckling curves available in the Eurocode EN1993-1–1 and developed for GMNI analyses and FEM-based design. The authors proposed Eq.(6) to be used to determine the required equivalent global imperfection for S235-S960. It was found that the dimensions of the box-section do not affect the required equivalent imperfections. The proposed formula is a function of $\varepsilon = \sqrt{\frac{235}{f_y}}$, the global slenderness ratio$\overline{\lambda}_g = \sqrt{\frac{Af_y}{N_{cr}}}$, and the imperfection

factor *α*. GMNI analysis using global imperfection obtained from the proposed formula yielded buckling resistances strongly agree with the buckling resistance obtained using the Eurocode curves with a maximum error of 2 %.

$$k_{globimp} = \frac{\varepsilon}{\alpha}\left(\overline{\lambda}_g^{-3.79} - 26.1\overline{\lambda}_g + 168\right) \quad (6)$$

2.2.2. Local imperfections

Local imperfections can be defined as buckles in a plate or twists of a flange or stiffener. The Eurocode EN1993-1–5 [4] states that the equivalent geometrical imperfections maybe be used unless a more refined analysis of the geometrical imperfection is done. The geometrical imperfections may be based on the shape of the critical buckling modes of the plates with amplitudes given in the National Annex of 80 % of the geometric fabrication tolerances. In the case of using the local equivalent geometric imperfection, the Eurocode suggests an amplitude of a minimum of *a/200* or *b/200*, where *a* or *b* is the shorter span of the plate. The buckling shape can be used for plates or subpanels with the mentioned amplitude. Johansson et al. [24] suggested the use of *b/420* as local imperfection with no residual stresses, or *b/500* with *0.1f$_y$* compressive residual stresses compared to the values of *a/200* that is suggested by the Eurocode to yield a close resistance to the Winter curve. It was mentioned that further studies could lead to further improvements.

Many researchers criticised the Winter-type buckling curve available in the EN1993-1–5 [4], and it was proven to be inadequate for welded box sections by Schillo et al. [2]. It was shown that the buckling curve available in Annex B of EN1993-1–5 [4] and the local buckling curve of Schillo et al. [2] show a better estimation of the local buckling capacity of square box-sections. The available local equivalent imperfection factor was suggested based on the Winter-type curve. As more accurate buckling curves are available, new local buckling imperfections must be suggested and calibrated to these buckling curves. Therefore, Radwan and Kövesdi [6] performed a large calibration parametric study to find the appropriate local imperfection factors based on the buckling curve available in Annex B of EN1993-1–5 [4] and the research performed by Schillo et al. [2]. Both equivalent geometrical imperfections and geometrical imperfections to be applied with residual stresses were back-calculated by the authors for both buckling curves. It was found that the local geometrical imperfection to be applied to the plates depends on the yield strength (*f$_y$*), and the relative slenderness ratio of the analysed cross-section (*$\overline{\lambda}_p$*). It was found that larger imperfections are needed for sections made of higher yield strength to yield the local buckling curve capacity, as the same buckling curve is used for all materials and increasing the yield strength results in an increased reduction factor (which is independent of the yield strength). Therefore, larger imperfections are to be applied, resulting in the same buckling resistance as predicted by the buckling curve developed by Schillo et al. [2]. The best-fit approximation for the calibrated equivalent geometric imperfection is given by Eq. (7), where *$\overline{\lambda}_p$* is the local plate slenderness ratio calculated by Eq. (6), *f$_y$* is the nominal yield strength of the analysed steel material. The imperfection factor is equal to $\frac{b}{f_{0.local}}$, *b* is the plate width.

$$f_{0,local} = \begin{cases} \frac{1}{\overline{\lambda}_p^{2.2}} \cdot (200 - 0.2 \cdot f_y), & \overline{\lambda}_p \leq 1.35 \\ \frac{1}{\overline{\lambda}_p} \cdot (160 - 0.2 \cdot f_y), & \overline{\lambda}_p > 1.35 \end{cases} \quad (7)$$

The authors also perform statistical evaluations on a large numerical database. Results prove that a constant value imperfection scaling factor *b*/125 would yield the best-fit buckling resistance, on average, according to the buckling curve developed by Schillo et al. [2] using FEM-based design [42].

2.3. Executed research strategy

As shown in the literature review, further investigations of the interaction behaviour between global and local buckling are needed as the current design procedures are not accurately estimating the capacity of steel box-section columns subjected to pure compression [2,3,14]. Furthermore, new local and global equivalent geometrical imperfections should be developed for the GMNI analysis to aid the FEM-based design process. To cover the shortcomings of the previous investigations, considering the interaction buckling, the authors developed new local imperfections on a large slenderness range. It was found that the value of the local imperfections significantly varies along with the local slenderness range. However, for the local imperfections, reliable values fitting to the buckling curves have just been developed by the authors [6], which are applied here to determine the interaction buckling resistance. The global imperfections and residual stresses for box-section columns are generally agreed upon and accepted by researchers in the past. Another shortcoming addressed in this study is the use of the Winter-type buckling curve in EN 1993–1–5[4] for the estimation of the buckling resistance, which was proved to be overestimating the buckling resistance of square box-sections, where the Annex B curve of EN1993-1–5[4] is used instead. The effect of utilisation of this buckling curve is shown in this study, as it was not investigated before. This buckling resistance obtained with this buckling curve is considered as the controlling and accurate buckling resistance. Two numerical parametric studies are performed to determine the combination of equivalent local and global imperfections. Three additional parametric studies are performed to test the applicability of the reducing factor for the accompanying imperfection if a leading imperfection is chosen. Table 1 shows a summary of all the used imperfections in this research.

The following research program is executed and presented in the current paper:

1. Suitable local geometric imperfection is applied to control the local buckling capacity according to Annex B curve of EN 1993–1-5[4], the used imperfection magnitudes vary depending on the *f$_y$* and *$\overline{\lambda}_p$* of each cross-section under study, as described in [6], with a maximum limit of the imperfection of ± b/125 as a maximum allowable imperfection specified by European manufacturing tolerance.
2. A global imperfection of L/1000 with applied residual stresses is used to control the global buckling capacity, as proposed in previous studies [3,24].
3. The development and validation of a numerical model based on available tests in the international literature.
4. A numerical parametric study is performed on a large range of global and local slenderness ranges to determine the local, global and interaction buckling resistance.
5. A numerical parametric study is carried out to back-calculate the equivalent global imperfection if the leading imperfection is the local equivalent imperfection.
6. A numerical parametric study is carried out to back-calculate the equivalent local imperfection if the leading imperfection is the global equivalent imperfection.

Table 1
Summary of local and global imperfections used in this study:

Imperfection Type	Residual stresses applied	Residual stresses not applied
Global Imperfection	*Memberlength(L)* / 1000	Somodi et al.[23] Eq. (8)
Local Imperfection	Radwan and Kövesdi [6] Calibrated imperfections to Annex B curve that depend on *f$_y$* and *$\overline{\lambda}_p$* with a maximum imperfection of ± b/125	Radwan and Kövesdi [6]Eq. (9)

7. An additional numerical parametric study is carried out to investigate three optional combinations of local and global geometric imperfections using the design rules of the EN 1993–1-5[4], applying one leading and one accompanying imperfection with 70 % magnitude.

3. Numerical model development and verification

3.1. Development of the numerical model

A four-node full thin shell model is used to develop the numerical model using Ansys finite element software [25], as shown in Fig. 1. Geometrical and material nonlinear analyses (GMNIA) are used to determine the buckling capacity. Half sin-wave imperfections are applied for the global and local buckling-type imperfections. The number of the half sin-waves for the local buckling is considered as an integer number resulting from dividing the length (L) of the plate by its width (b). The half sin-waves are applied on all four sides of the column with amplitudes having opposite signs for adjacent sides as shown in (Fig. 1. a). The outward imperfections are considered positive. The global imperfection is defined as one large half sin-wave along the full length of the column, as shown in (Fig. 1.b). To study the interaction of columns, both the global and the local imperfections are defined at the same time, as shown in (Fig. 1.c).

The boundary conditions and loads are applied to two additional master nodes created at the column section's geometrical centre. The nodes at the end cross-sections are connected to these master nodes using rigid diaphragms to link all 6 DOFs and transfer the forces. The master node of one side of the column is restrained against translation in the global (UX, UY, UZ) directions and against rotation along the longitudinal axis (ROTZ). The other master node is restrained in (UX, UY) and (ROTZ) only to allow the application of the compressive force of the column.

Different proposals for material models of normal strength steel (NSS) are available in the international literature. The material model shown in Fig. 2 is applied, which is a quad-linear material model developed for hot-rolled steel that is accurately able to capture the strain hardening behaviour of the normal strength steel (NSS) as proposed by Yun and Gardner based on a large number of coupon tests[26].

This material model uses a set of coefficients to define the stress–strain relationship and is used in Ansys as a multilinear inelastic material
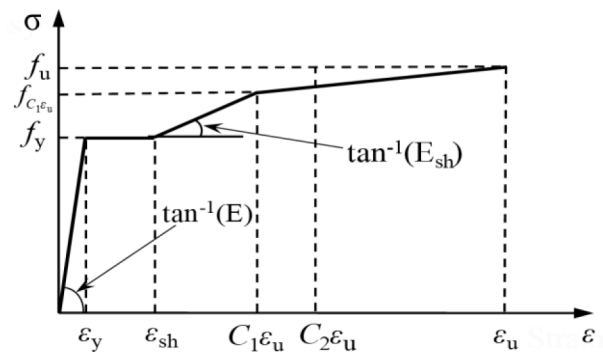

Fig. 2. The applied material model for NSS according to prEN 1993-1-14 [27].

model. Table 2 shows the list of the coefficients that are needed to define the model, including yield strain $\varepsilon_y = f_y/E$, strain hardening strain ε_{sh}, and strain hardening modulus E_{sh}, $A = 0.2$ which is the elongation after fracture, C_1 "cut-off" strain coefficient defined to prevent over-predictions strength, and C_2 to determine the slope of strain hardening E_{sh}. A modulus of elasticity of E = 210000 MPa and a Poisson's ratio $v = 0.3$ are used for all numerical tests in this research program.

Several researchers [28 29] suggested residual stress models to apply the residual stress of welded box-sections in the numerical model, as the effect of residual stress was proven to be significant and can lead to premature yielding and loss of stiffness of slender plates under compression. A frequently used residual stress model, which was proven to be reliable and leads to a good estimation of buckling resistance is shown in Fig. 3. (σ_t) and the positive sign represent tensile residual stress, while (σ_c) and the negative sign represent compressive residual stress. The shown model follows the recommendations of the European Convention for Constructional Steelworks (ECCS) [30] and the draft Eurocode prEN1993-1–14 [27]. For NSS, the compressive stress is considered according to Table 3, and tensile residual stress is equal to the yield strength of the material under study. The parameters a and b in Fig. 3 define the regions subjected to tensile stress near the corners of the section. The vast majority of the sections under this study are slender sections with an H/t ratio larger than 40 to study class 4 sections that experience the interaction buckling, assuming light welding.
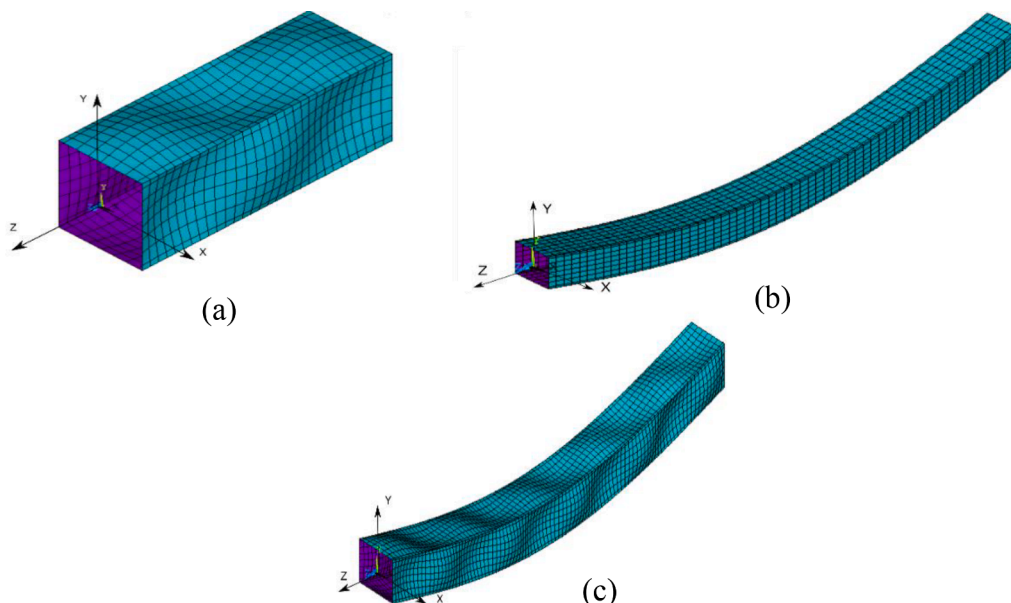

Fig. 1. A) local, b) global, and c) interaction definitions of imperfections.

Table 2
The parameters of the applied material model.

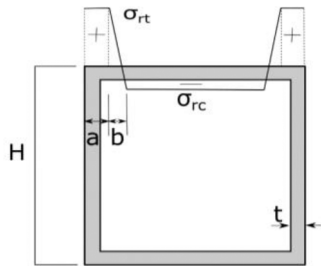|	f_y [MPa]	f_u [MPa]	ε_{sh} [-]	ε_u [-]	$C1$ [-]	$C2$ [-]	E_{sh} [MPa]	$C1 \cdot \varepsilon_u$ [-]	$f_{C1\varepsilon u}$ [MPa]
S235	235	360	0.01	0.208	0.287	0.43	1578	0.06	313
S355	355	510	0.015	0.182	0.31	0.448	2310	0.057	451
S460	460	540	0.03	0.089	0.505	0.604	3407	0.045	510

Fig. 3. The residual stress model for welded box-section columns[6].

3.2. Validation and verification of the numerical model

Choosing an appropriate mesh size that yields an accurate resistance without being numerically expensive is crucial for performing large parametric studies as it saves time and resources. Therefore, a mesh sensitivity analysis is performed for the smallest and largest plate widths available in this study. It was found that 16 elements along the plate width yielded an accurate result with an error of less than 1 % from the smallest mesh size, as shown in Fig. 4. The shown case is an S500 box section with a width b of 160 mm, a thickness t of 4.1 mm and a length L of 1400 mm. A mesh size of 10 mm representing 16 elements is chosen for the case shown. All other cases are controlled to have a similar width-to-elements number ratio. Experimental tests available in the international literature are used to validate the numerical model. In the current study, three research programs are used to validate the model. Four samples were taken from each research program. Different steel grades are tested, including S235, S500, S700, and S960. The material and residual stress models presented previously are used to validate the numerical model. The measured values of the columns understudy are used in the numerical model according to the experimental research programs. As previously justified, a global imperfection of $L/1000$ is applied in the numerical model, with the calibrated local geometrical imperfections and residual stress developed by the authors, presented in *Fig.15* of the previous research [6]. All the tested samples in the

validation process are available in Table 4. The mean and the CoV of the full sample set are equal to 0.99 and 0.061, respectively. The majority of the samples showed a high agreement with the numerical model with a 5 % difference, as shown by *Fu,num/Fu,*exp column of Table 4. The larger differences can be due to the unintended eccentricities in the experimental tests. Two samples are shown in Fig. 5 to compare the numerical and experimental results. The figure on the left shows a test result taken from a research program done by Khan et al. [9]. The figure on the right-hand side is taken from the research program done by Schillo and Feldmann [8]. Both samples show a good estimation of the behaviour and the buckling capacity of the experimental tests. The first sample experiences interaction buckling, and the second sample experiences pure local buckling.

This proves the applicability and reliability of the numerical model to capture the different types of buckling under study. Fig. 6 shows the interaction buckling mode, illustrating the experimental test, the deformations and the von-Mises stresses for a specimen taken from the research program done by Khan et al. /S700-150–4.92–2512/ [9].The validation process shows the numerical model predicts reliable results and the numerical model used by the authors is highly accurate.

4. The evaluation strategy and sections properties

4.1. The evaluation strategy

In order to show that the numerical model can capture the failure modes reliably, the two extreme cases: (i) pure local (ii) pure global

Table 3
Residual stress model parameters according to ECCS [30].

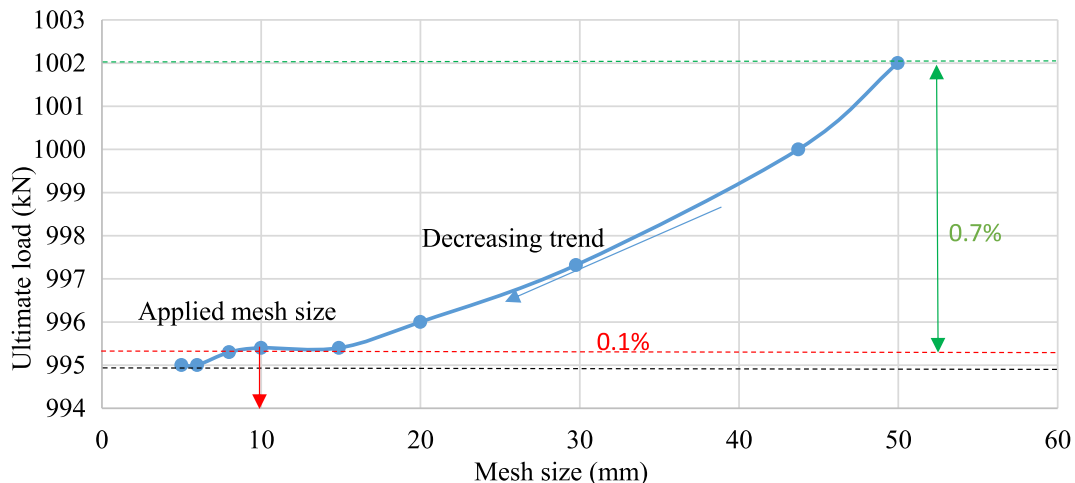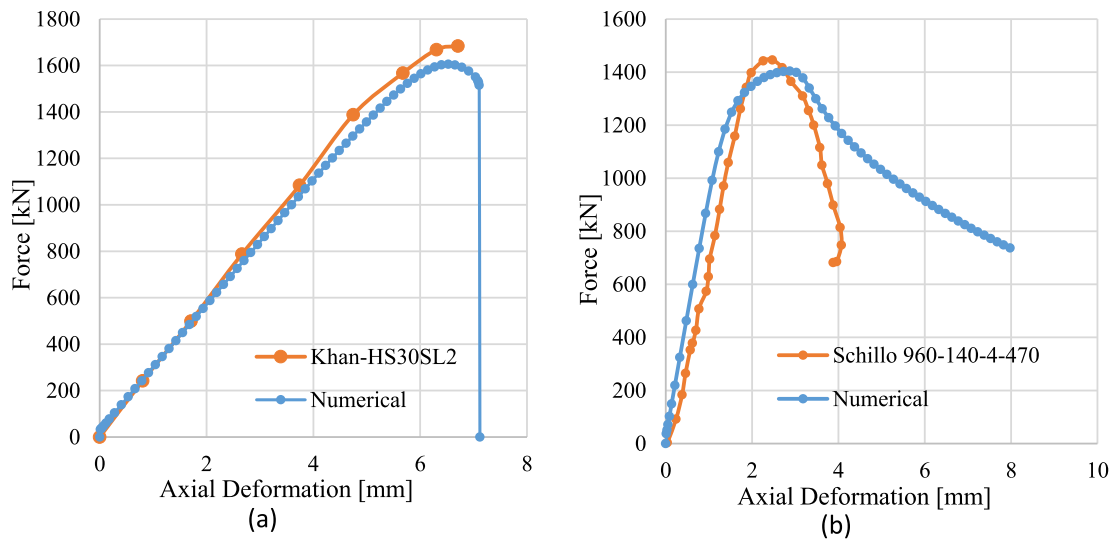| H/t	Welding type	σ_{rt}/f_y	σ_{rc}/f_y	a	b
10	–	1.0	−0.60	0	–
20	Heavy weld	1.0	−0.82	3 t	3 t
20	Light weld	1.0	−0.29	1.5 t	1.5 t
40	Heavy weld	1.0	−0.29	3 t	3 t
40	Light weld	1.0	−0.13	1.5 t	1.5 t

Fig. 4. Mesh sensitivity analysis.

Table 4
Results of the numerical validation process.

Steel grade	λ_g	λ_p	b (mm)	h (mm)	t (mm)	L (mm)	f_y (MPa)	f_u (MPa)	Imp. Sc. fa. (f_{local})	$F_{u,exp}$ (kN)	$F_{u,num}$ (kN)	$\frac{F_{u,num}}{F_{u,exp}}$
S235	0.37	0.71	80	80	2	1100	261	360	2130	159	150.75	0.95
S235	0.47	0.71	80	80	2	1500	261	360	2130	140	141.69	1.02
S235	0.59	0.71	80	80	2	1850	261	360	2130	143	134.51	0.94
S235	0.50	0.71	80	80	1.4	1850	261	360	566	72	72.31	1.01
S500	0.33	1.06	159.75	159.5	4.1	1599	562	640	633	880.3	948	1.08
S500	0.37	1.07	160	159.25	4	1800	562	640	606	883.9	925	1.05
S500	0.40	1.08	160	159	4	2000	562	640	599	858.2	899	1.05
S500	0.44	1.08	159.25	159.25	4	2198	562	640	600	828.9	889	1.07
S700	0.28	1.22	199	199	4.9	1512	762	819	147	1733	1735	1.00
S700	0.45	0.90	149	149	4.9	1512	762	819	515	1800	1698	0.94
S700	0.57	0.74	125	125	4.9	1512	762	819	400	1659	1593	0.96
S700	0.45	1.22	199	199	4.9	2512	762	819	125	1598	1626	1.02
S960	0.15	1.25	137	137	3.9	470	980	1024	125	1444.1	1298	0.90
S960	0.23	1.17	136	136	4.2	728	980	1024	178	1400.4	1383	0.99
S960	0.42	1.24	137	137	4	1299	980	1024	132	1390.5	1223	0.88
										Mean		0.99
										CoV		0.061

Fig. 5. The measured and numerically obtained load-deformation curves: a) Khan et al. test specimen S700-150–4.92–2512[9] and b) Schillo and Feldmann test specimen S960-140–4-470[8].

buckling, are investigated separately. After that, the interaction behaviour is analysed using the same numerical model applying the suggested imperfections combination. In previous research [6], the authors studied the local buckling behaviour of welded box-section columns in a detailed manner. Here only the final results and the calculated buckling reduction factors are shown. Fig. 7.*a* shows the results of the local buckling study, where the local slenderness ratios are shown on the horizontal axis and the buckling reduction factors on the vertical axis. The two buckling curves are (i) the EN1993-1–5 Annex B buckling curve, according to Eq.(10), which is proposed by the Eurocode and (ii) the buckling curve developed by Schillo et al. [2], according to Eq.(11), which is found to be more reliable than the Winter-type curve[6,5]-[31] for welded box-sections. The buckling curve developed by Schillo et al. [2] was checked and statistically evaluated using a large test database collected from the international literature, shown here by the red curve in Fig. 7.*a*. In previous research [6], the authors calibrated local imperfections to the Annex B curve, and it was shown that if these imperfections are applied with the manufacturing tolerance [16] of $b/125$ as the largest imperfection, these imperfections provide accurate resistances to the test based buckling curve, developed by Schillo et al.[2],

in combination with residual stresses, as shown by the black circles in Fig. 7.*a*. Therefore, these imperfections are considered accurate and can be used to estimate the local buckling capacity of welded box-section columns.

$$\rho = \frac{1}{\phi_p + \sqrt{\phi_p^2 - \overline{\lambda}_p}}$$

(10)

$$\phi_p = \frac{1}{2}\left(1 + 0.34\left(\overline{\lambda}_p - 0.7\right) + \overline{\lambda}_p\right)$$

$$\rho = 2.235 \bullet e^{-1.582 \bullet \overline{\lambda}_p} + 0.288$$

(11)

In the case of sections dominated by global buckling, the application of $L/1000$ geometric imperfections and residual stresses in the numerical model is widely accepted to estimate the global buckling capacity. Fig. 7.*b* shows that the numerical analysis performed with these conditions provides flexural buckling resistance close to the buckling curve "b" of the EN 1993-1-1, which is the curve used to estimate the flexural buckling of welded box-section columns. Numerical simulations performed using the $L/1000$ and the application of residual stresses provide
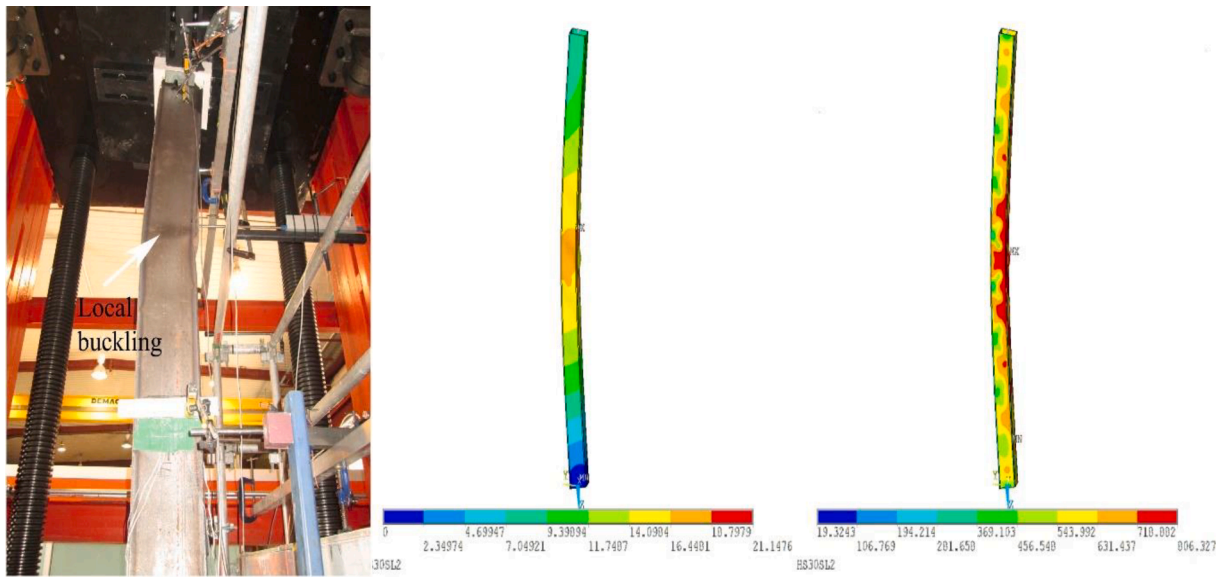
Fig. 6. The numerically obtained failure mode for interaction buckling at the final loading step for Khan et al. test specimen S700-150–4.92–2512[9]; a) experimental test[9],b) deformed shape, b) Von-Mises stresses.
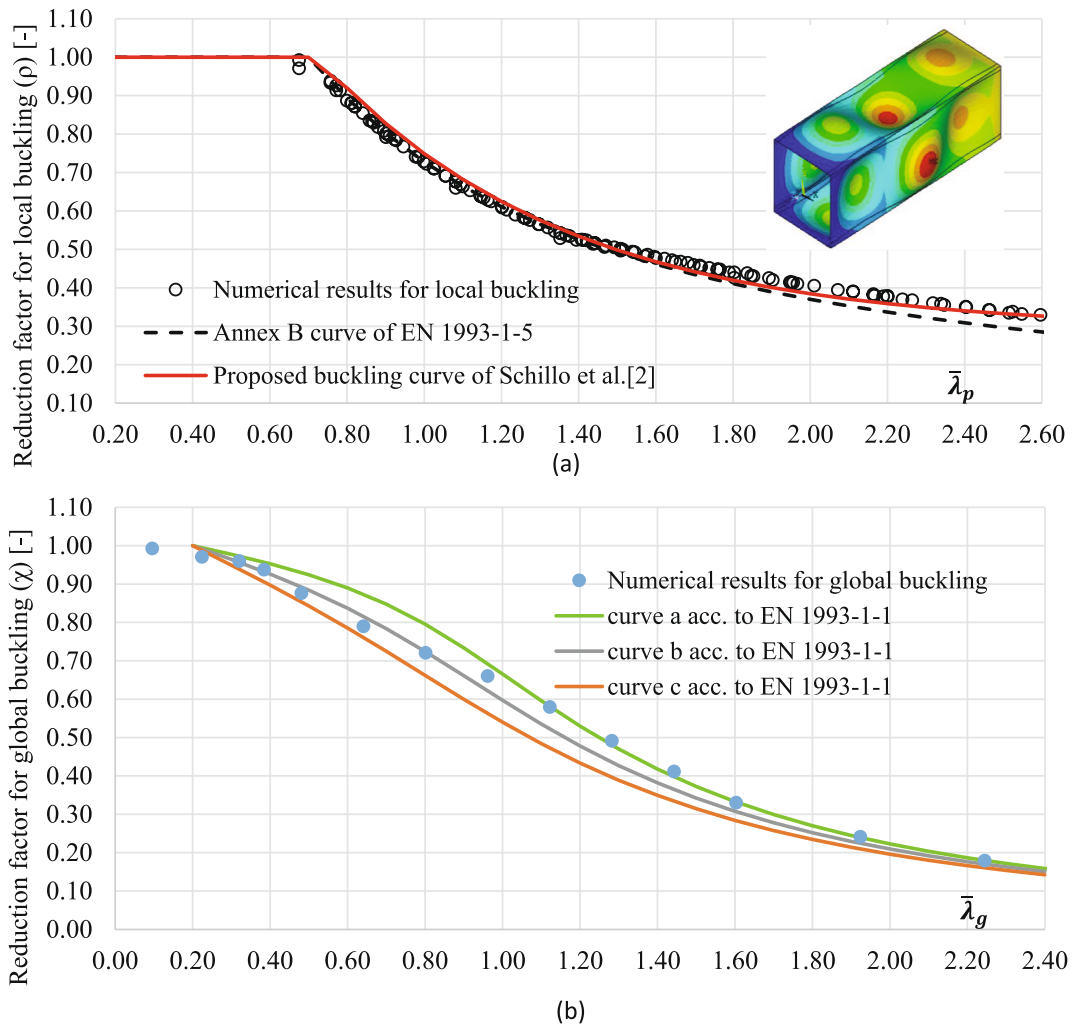

Fig. 7. A) numerically obtained local buckling resistances compared to buckling curves. b) numerically obtained global buckling resistances compared to buckling curves.

an average estimation of the buckling curve b with a mean ratio $\frac{F_{numerical}}{F_{bcurve}}$ of 1.04 and a CoV value of 0.055.

As the previously discussed global and local imperfections are able to provide accurate results for pure local and global buckling, applying these imperfections for samples experiencing interaction buckling will yield accurate results, too, as was shown previously by the authors [32]. Therefore, in the current research program, the resistance obtained using the combination of L/1000 and the previously developed local imperfections with a manufacturing tolerance of b/125 and applied residual stresses is considered as the target resistance. This target resistance will be used further on to find the required equivalent global and local geometric imperfection combinations that can be applied in FEM-based design.

The equivalent global and local imperfection will be determined by applying the proposed criterion of the prEN 1993-1-14; thus, one leading imperfection is selected, and the necessary magnitude for the accompanying imperfections is determined. Two parametric studies are performed. The first parametric study is used to determine the equivalent global imperfection by assuming leading local imperfection (always considered with 100 %) and calibrating against the target resistance to determine the accompanying global imperfection, as shown in Fig. 8, and according to Eq.(12). The equivalent local imperfections calibrated for buckling curve, developed by Schillo et al.[2], is used as local imperfections, applied as (b/f_{local}), where b is the width of the plate and f_{local} according to Eq.(7). The equivalent global imperfection is the buckling length divided by the global imperfection scaling factor (L/f_{global}).

$$e_0 = 100\% \bullet e_{local} + x\% \bullet e_{global} \qquad (12)$$

Fig. 8 shows the calibration of the equivalent global imperfection, where the x-axis shows the applied equivalent global imperfections. The y-axis shows the obtained buckling resistance of the GMNI analysis. The calibration is done by analysing multiple numerical models with different equivalent global imperfections for each cross-section with specific global and local slenderness ratios and comparing the obtained curve with the previously obtained target resistance value (presented by the horizontal line). The intersection point of the curve and the horizontal line represents the required global equivalent geometric imperfection that can be used by the designer.

The second parametric study is performed to determine the equivalent accompanying local imperfection by considering the global imperfection as the leading imperfection (always considered with 100 %) and calibrating against the target resistance according to Eq. (13). The leading global imperfection is defined as $e_{0,global} = L/f_{global}$ is defined according to the formula developed by Somodi et al.[23], with f_{global} according to Eq. (6), for pure global buckling and $x\%$ $e_{0,local}$ is the value to be determined. The equivalent local imperfection factor is considered as (b/f_{local}), where b is the smaller width of the plate and f_{local} is the local

equivalent imperfection scaling factor to be determined.

$$e_0 = x\% \bullet e_{local} + 100\% \bullet e_{global} \qquad (13)$$

A similar technique is used to calibrate and find the accompanying equivalent local imperfection scaling factor, as shown in Fig. 8.

Providing equivalent global and local imperfection combinations simplifies performing GMNI analysis for designers by avoiding the modelling request of residual stresses, which can be challenging in some cases. Furthermore, the combination rule for the global and local imperfection ensures that the effect of the residual stresses is not duplicated, leading to conservative buckling resistance.

4.2. Sections properties used in the numerical study

A large parametric study is used to create a database for interaction buckling resistances. This database is used to back-calculate equivalent global and local imperfection combinations. In this study, the vast majority of cross-sections have an *H/t* ratio larger than 40 with a global slenderness ratio $(\overline{\lambda}_g)$ larger than 0.2 and a local slenderness ratio $(\overline{\lambda}_p)$ larger than 0.7. Only square box-section columns are studied within the current research covering a wide range of width-to-thickness ratios and cross-section dimensions. The applied geometries and section dimensions are given in Table 5.

Table 5
Geometrical properties of the analysed cross-sections.

	$b = h$ [mm]	Thickness values [mm]	Lengths [mm]
1	200	2.0; 2.5; 3.0; 3.5; 4.0; 4.5; 5.0; 5.5; 6.0; 6.5;	750;1750;2500;3000;3750;5000; 6250;7500;8750;10000;11250; 12500;15000;17500;20000
2	250	2.0; 2.25; 2.5; 2.75; 3.0; 3.25; 3.5; 4.0; 5.0; 6.0; 7.0; 8.0	
3	300	2.75; 3.0; 3.5; 4.0; 4.25; 4.5; 4.75; 5.0; 5.25; 5.5; 5.75; 6.0; 6.5; 7.0; 8.0; 9.0	
4	350	2.75; 3.0; 3.5; 4.0; 4.5; 5.0; 5.5; 6.0; 6.5; 7.0; 8.0; 9.0; 10.0	
5	400	3.5; 3.75; 4.0; 4.25; 4.5, 4.75; 5.0; 5.5; 6.0; 6.5; 7.0; 8;0	
6	450	3.75; 4.0; 4.25; 4.5; 4.75; 5.0; 5.25; 5.5; 5.75; 6.0; 6.5; 7.0; 8.0; 9.0; 10.0; 11;0	

All geometries are investigated using steel grades of:
NSS: S235, S355, S460
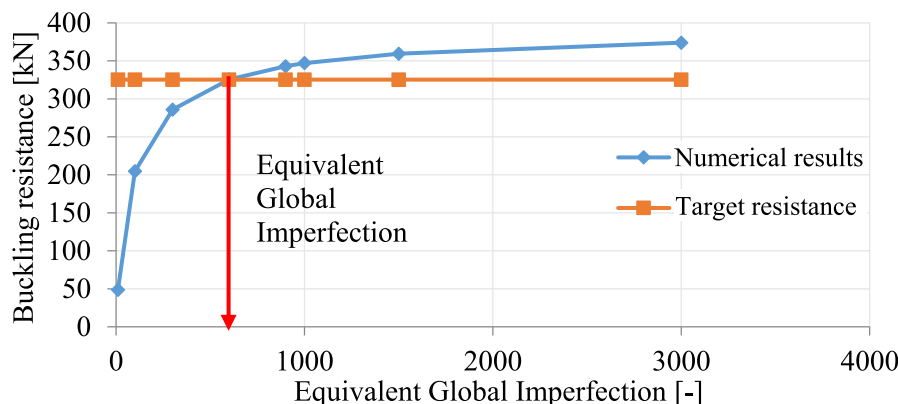
Fig. 8. Results of imperfection sensitivity study and determination of necessary imperfection scaling factor for the accompanying global imperfection.

5. Results of the parametric studies

5.1. Equivalent global geometrical imperfection

Carrying out the previously mentioned procedures for a wide range of global and local slenderness ratios results in finding the accompanying equivalent global imperfections for all the points along the studied global and local slenderness ranges (local imperfection was the leading imperfection taken with its 100 % value according to Eq. (7)). It was noticed that the differences between the accompanying global imperfections for the studied steel types are relatively small. Therefore, one formula is used to estimate the equivalent global imperfection to all the analysed steel grades given by Eq. (15). Matlab was used to derive the formula using custom functions for the segments of the proposed formula, where the general form of the formula is given to Matlab to yield best-fitting coefficients. The residuals were determined to minimize the errors. The formula for accompanying equivalent global imperfection is presented as the ratio f_{int}/f_{glob}, where f_{glob} is the imperfection scaling factor for pure global buckling obtained using Eq.(6) and f_{int} is the accompanying imperfection scaling factor. The proposed formula is a function of both the local and the global slenderness ratios, and it has clear physical background. Fig. 9 shows the proposed formula that can be used to estimate the accompanying equivalent global imperfection scaling factor, where the x-axis shows the local slenderness $\bar{\lambda}_p$ and the y-axis shows the f_{int}/f_{glob} ratio for different global slenderness ratios $\bar{\lambda}_g$. It can be seen for $\bar{\lambda}_p < 0.7$ the required equivalent accompanying global scaling factor is equal to 1.0 as there is no interaction before this value. Around the range $\bar{\lambda}_p = 0.9$ and 1.1 the ratio f_{int}/f_{glob} is the largest (smallest imperfection) as in this region, the largest local imperfection was applied. For the range $\bar{\lambda}_p > 1.35$, the obtained imperfections are relatively large, meaning the residual stress effect is not covered by the leading local imperfection alone. It also can be noticed the f_{int}/f_{glob} ratio is larger as the global slenderness ratio $\bar{\lambda}_g$ is increased, where for stocky columns larger imperfections are needed to reach the target capacity.

The accompanying equivalent global imperfection for interaction buckling is presented in Eq.(14), where f_{int} is obtained using Eq.(15).

$$Equivalent\,global\,imperfection = \frac{L}{f_{int}} \qquad (14)$$

$$f_{int} = f_{glob} * \begin{cases} \bar{\lambda}_p \leq 0.7, 1 \\ 0.7 < \bar{\lambda}_p < 1, 1 + \frac{1.6*\bar{\lambda}_g + (1 + 7 \bullet \bar{\lambda}_g)}{0.3} \bullet (\bar{\lambda}_p - 0.7) \\ \bar{\lambda}_p > 1.0, 1.6 \bullet \bar{\lambda}_g + (1 + 7 \bullet \bar{\lambda}_g) \bullet \frac{1}{\bar{\lambda}_p(\max(4, 1 + 6\bar{\lambda}_g))} \end{cases}$$
(15)

The following calculations are presented to demonstrate the applied values for an average box-section column with a $\bar{\lambda}_g$ and $\bar{\lambda}_p$ of 1.0. The accompanying global scaling imperfection factor $f_{int} = 6.5 \bullet f_{glob}$. The value for $f_{glob} = 350$ is obtained using Eq.(6). The required accompanying imperfection is equal to $\frac{L}{6.5*350} = \frac{L}{2275}$ if local imperfections are also applied with their 100 % value, according to Eq.(7). The obtained benchmark result for mentioned slenderness range is equal to $\frac{L}{2206}$. The ratio of the fit to the benchmark result is 1.03.

5.2. Equivalent local geometrical imperfection

The calibration in the other direction is also done against the accurate buckling resistance obtained by modelling the residual stresses using the process shown in section 4.1. The study is performed for a wide range of global and local slenderness ratios as well as different types of steel, the local equivalent imperfection scaling factor for this wide range can be found. In this case, the global imperfection is taken as the leading imperfection having the 100 % value and the necessary local imperfection magnitudes are determined for all analysed column geometries. Fig. 10 shows the proposed accompanying equivalent local imperfection if Eq.(6) is applied as a leading global imperfection factor.

The x-axis shows the global slenderness ratio $\bar{\lambda}_g$ and the y-axis shows the f_{int}/f_{loc} ratio, where the f_{int} is the equivalent local imperfection scaling factor for interaction buckling and f_{loc} is the equivalent imperfection scaling factor for local buckling. It can be seen in Fig. 10 that the ratio f_{int}/f_{loc} follows a clear trend, where larger equivalent local imperfection (large f_{int}/f_{loc} ratio) is needed for sections with large local slenderness ratios and a smaller one is needed for sections with larger slenderness ratio (small f_{int}/f_{loc} ratio). This depends on the applied accompanying global imperfection used; sections with a large global slenderness ratio require a larger global imperfection factor, according to Eq. (6). Additionally, steel grades with higher yield strength require a larger global imperfection because Eq. (6) was calibrated for Eurocode buckling curves, which are independent of the yield strength. Only the global slenderness ratio depends on the yield strength (f_y); therefore, a higher global imperfection factor is needed to achieve the same
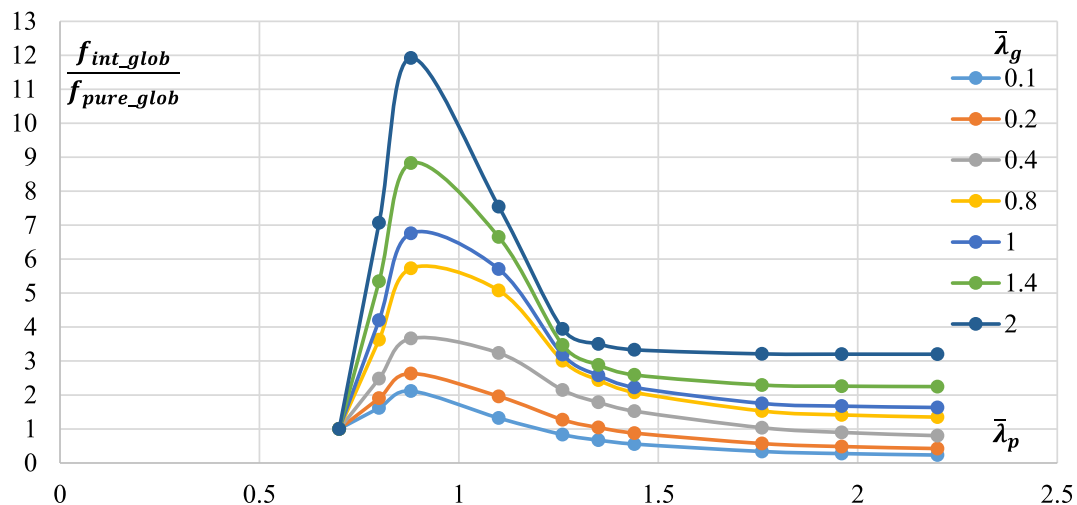

Fig. 9. The proposed model for accompanying global equivalent geometric imperfections.
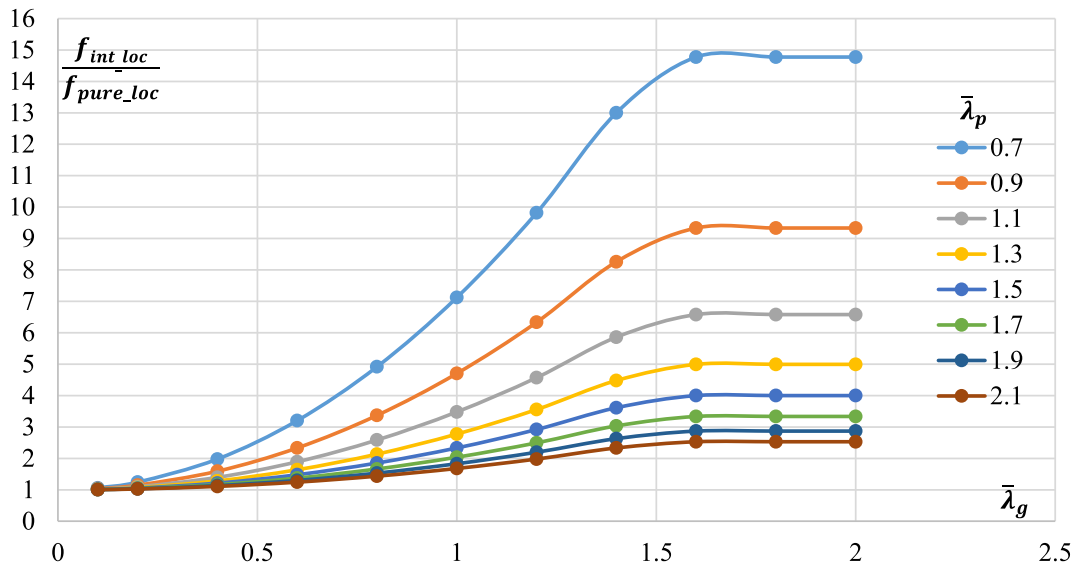
Fig. 10. The proposed model for accompanying local equivalent geometric imperfections.

resistance proposed by the Eurocode buckling curves. For the same global and local slenderness, the differences between the different types of steel grades are insignificant, and therefore one formula can be used to represent all three types of steel, according to Eqs. (16-17). The accompanying equivalent local imperfection for interaction buckling is presented in Eq.(16), where the f_{int} is according to Eq.(17).

$$Equivalent\ Local\ imperfection = \frac{b}{f_{int}} \qquad (16)$$

$$f_{int} = f_{loc} * \begin{cases} (1 + \overline{\lambda}_g^2 * 3 * \overline{\lambda}_p^{-2}, \overline{\lambda}_g \leq 1.5 \\ (1 + 6.75 * \overline{\lambda}_p^{-2}, \overline{\lambda}_g > 1.5 \end{cases} \qquad (17)$$

It is worth mentioning that this formula is always yielding a larger equivalent local imperfection scaling factors than the imperfection factors calibrated to the buckling curve for pure local buckling according to Eq. (7). The following calculations are presented to demonstrate the applied values for an average box section column with a $\overline{\lambda}_g$ and $\overline{\lambda}_p$ of 1.0. The accompanying local scaling imperfection factor $f_{int} = 3 \bullet f_{glob}$. The value for $f_{loc} = 110$ is obtained using Eq.(7). The required accompanying imperfection is equal to $\frac{b}{3*110} = \frac{b}{330}$. The obtained benchmark result for mentioned slenderness range is equal to $\frac{b}{345}$. The ratio of the fit to the benchmark result is 0.96. It is worth mentioning that for the range $\overline{\lambda}_p < 0.9$ and $\overline{\lambda}_g > 0.8$ the obtained equivalent local imperfection is always smaller than $b/500$. For this range, if only the global imperfection is applied according to Eq.(6), the buckling capacity is overestimated by less than 5 %.

5.3. Statistical evaluations of the calibrated imperfection combinations

This section presents the reliability assessment executed following the method of the EN1990 Annex D [33] to check the validity and accuracy of the proposed imperfection formulas. As shown previously, the target capacity, determined using the developed combination of residual stresses and imperfections by the authors[6], provides an accurate estimation of the interaction buckling resistance of welded square box-sections. This target capacity is considered as the experimental results r_e in this reliability assessment study. The theoretical buckling capacity r_t is the resistance obtained using numerical analyses utilizing the proposed imperfection formulas introduced in sections 5.1 and 5.2. Annex D of EN1990[33] presents a set of steps that must be followed to find suitable partial safety factors. The target value for the corrected partial

safety factor γ_M^* for member stability is equal to 1.0 for buildings and 1.1 for bridges. The first step is comparing the experimental r_e and the theoretical r_t resistances, as shown in Fig. 11.

The next step is determining the model uncertainties by determining the mean value correction factor b and the error term δ_i for each experimental resistance value, according to Eqs. (18-19). Then the variance s^2 and the coefficient of variations V_δ can be determined using Eqs. (20-23). The coefficient of variation V_δ is used to measure the variabilities in estimating the resistance using the proposed theoretical values.

$$b = \frac{\sum r_{e,i} \bullet r_{t,i}}{\sum r_{t,i} \bullet r_{t,i}} \qquad (18)$$

$$\delta_i = \frac{r_{e,i}}{b \bullet r_{t,i}} \qquad (19)$$

$$\Delta_i = ln(\delta_i) \qquad (20)$$

$$\overline{\Delta} = \frac{1}{n} \sum_{i=1}^{n} \Delta_i \qquad (21)$$

$$s^2 = \frac{1}{n-1} \sum_{i=1}^{n} (\Delta_i - \overline{\Delta})^2 \qquad (22)$$

$$V_\delta = \sqrt{(\exp(s^2) - 1)} \qquad (23)$$

The next step is determining the uncertainties due to the basic variables. In this study, the considered basic variables are the material strength f_y, the plate width b, the thickness t, and the length L. The coefficients of variations for these variables are summarized in Table 6 based on the recommendations of Johansson et al. [34] and JCSS code [35]. V_{rt} is the general coefficient of variations (CoV). It includes all the CoVs of the basic variables. The V_{rt} can be determined in two methods, either using Eq.(24) or Eq.(25), depending on whether the basic variables are independent or dependent. Eq.(26) or Eq.(27) can be used to determine the combined CoV of the model, where Eq.(26) is used if the V_{rt} and V_{xi} of the basic variables are small.

$$V_{rt}^2 = \sum_{i=1}^{j} V_{Xi}^2 \qquad (24)$$
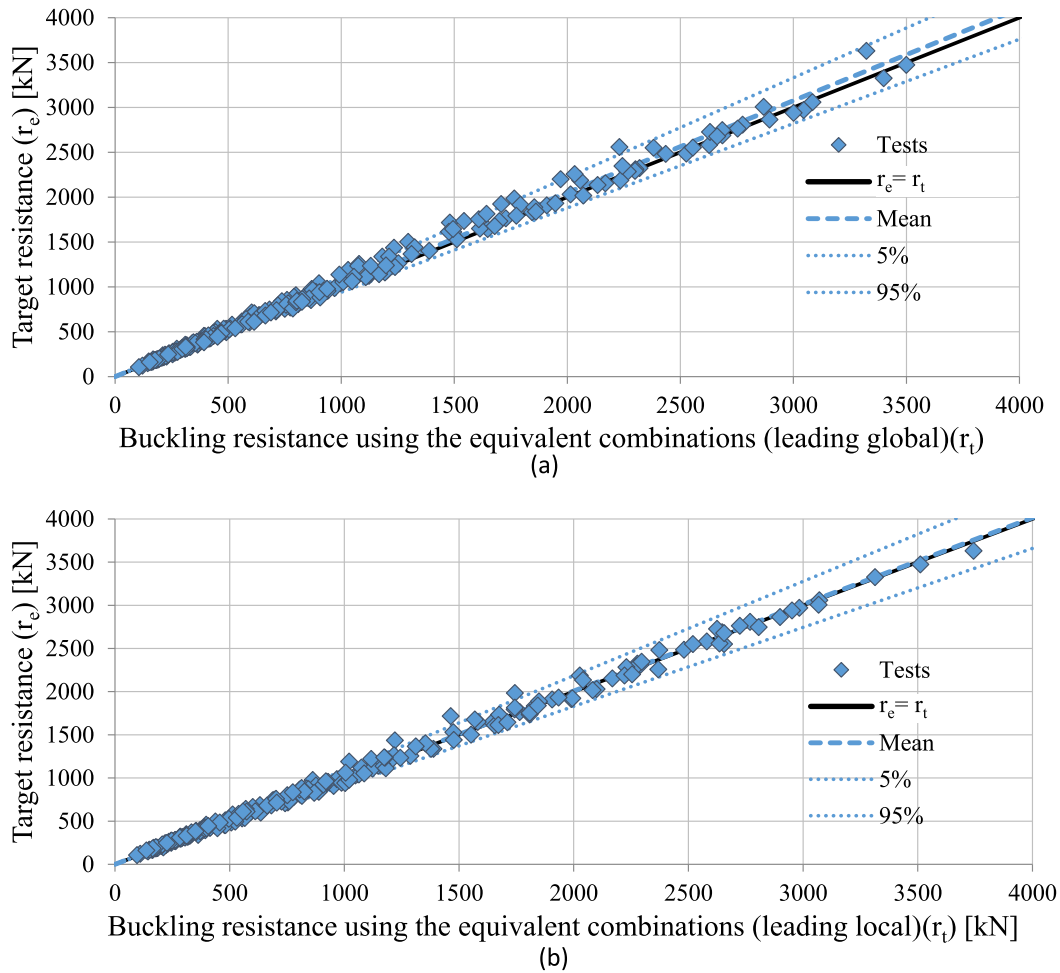
Fig. 11. The relationship between the target resistance r_e (experimental) and the buckling resistance from numerical analyses using the obtained combination of imperfections r_t (theoretical). a) using leading global and accompanying local. b) using leading local and accompanying global.

Table 6
Coefficient of variations for each parameter based on Johansson et al. [34] and JCSS recommendations[35].

Parameter	Coeff. of Variation (CoV)
Plate thickness V_t	0.05
Plate width V_b	0.005
Yield strength V_{fy}	0.07
Length L	0.005

$$V_{rt}^2 = \frac{VAR\left[g_{rt}\left(X_-\right)\right]}{g_{rt}^2\left(X_{-m}\right)} = \frac{1}{g_{rt}^2\left(X_{-m}\right)} \times \sum_{i-1}^{j} \left(\frac{\partial g_{rt}}{\partial X_i} \times \sigma_i\right)^2 \qquad (25)$$

$$V_r^2 = V_{rt}^2 + V_\delta^2 \qquad (26)$$

$$V_r^2 = \left(1 + V_\delta^2\right)\left(1 + V_{rt}^2\right) - 1 \qquad (27)$$

The partial safety factor γ_M is determined according to Eq.(28), where r_k and r_d are the characteristics and the design values of the resistance determined by Eq.(29) and Eq.(30), respectively. k_∞, kn, $k_{d\infty}$, and $k_{n,d}$ are determined using Table D1 and D2 of EN1990[33]. Qrt, Q_δ and Q are determined using Eqs. (31-33). α_{rt} and α_δ are determined using Eqs. (34-35).

$$\gamma_M = \frac{r_k}{r_d} \qquad (28)$$

$$r_k = b.g_{rt}(X_{-M})\exp(-k_\infty\alpha_{rt}Q_{rt} - k_n\alpha_\delta Q_\delta - 0.5Q^2) \qquad (29)$$

$$r_d = b.g_{rt}\left(X_{-M}\right)\exp(-k_{d\infty}\alpha_{rt}Q_{rt} - k_{d,n}\alpha_\delta Q_\delta - 0.5Q^2) \qquad (30)$$

$$Q_{rt} = \sqrt{\ln\left(V_{rt}^2 + 1\right)} \qquad (31)$$

$$Q_\delta = \sqrt{\ln\left(V_\delta^2 + 1\right)} \qquad (32)$$

$$Q = \sqrt{\ln\left(V_r^2 + 1\right)} \qquad (33)$$

$$\alpha_{rt} = \frac{Q_{rt}}{Q} \qquad (34)$$

$$\alpha_\delta = \frac{Q_\delta}{Q} \qquad (35)$$

The corrected partial safety factor γ_M^* can be determined using the nominal values of the basic variables. The method is presented by Taras and da Silva [36], da Silva et al. [37], Walport et al. [22], Heinisuo [38], Taras and Huemer [39] and Schillo et al. [2]. Using nominal values will generally lead to a more accurate estimation of the partial safety factor for the analysed resistance model. A different method is also available in the literature to determine the partial safety factor γ_M^* by considering the difference between the nominal resistances and the difference between the mean and the characteristic resistance values. The coefficient (Δk) is

Table 7
Overstrength factors for different steel types based on the recommendations of Schillo et al. [2].

Grade	235	355	460
f_{ymean}/f_{ynom}	1.25	1.2	1.15

a modification factor equal to the mean value of the resistance using the nominal input parameters over the characteristic value of resistance. Q_{fy} is equal to 0.07 based on JCSS recommendations [35].

$$\gamma_M^* = \Delta k \bullet \gamma_M \tag{36}$$

Where:

$$\Delta k = \frac{r_{nom}}{r_k} = \frac{\exp(-2Q_{fy} - 0.5Q_{fy}^2)}{b \bullet \exp(-k_\infty Q - 0.5Q^2)} = \frac{0.867}{b \bullet \exp(-1.64Q - 0.5Q^2)} \tag{37}$$

Afshan et al.[40] developed a method based on the procedures of Annex D of EN 1990[33] to determine the basic variable's uncertainties. Taking the dependency of the basic variables into account will lead to lower basic variables uncertainties V_{rt}. The buckling resistance of members experiencing local buckling depends on the basic variables, including the yield strength f_y, the plate width b, the thickness t, and the length L. The dependency of the member resistance on the basic variables can be derived for each numerical simulation using different exponents c, d, e, and f that are applied to the basic variables. The values of these exponents are equal to $\ln(N_{1.05Xi}/N_{Xi})/\ln(1.05X_i/X_i)$, where X represents the basic variable. The $N_{1.05fy}$, $N_{1.05t}$, $N_{1.05L}$, and $N_{1.05b}$ represent the buckling resistances obtained from numerical analyses with yield stress f_y, thickness t, the Length L, and width b multiplied by 1.05, respectively. The N_{fy}, N_t, N_L, and N_b are the obtained buckling resistances. In this method, the overstrength factors ($f_{y,mean}/f_{y,nom}$) are utilized to yield a more reliable corrected safety factor γ_M^*. The overstrength factors are listed in Table 7.

Based on the recommendations of Afshan et al.[40] and Tuezney et al.[41], the following modifications are adopted to account for the dependent variables and the overstrength factors, where the γ_M^* is determined according to *Eq. (38)*.

$$\gamma_M^* = \frac{\sum r_{n,i}^2}{\sum r_{n,i} \bullet r_{d,i}'} \tag{38}$$

$$r_{d,i}' = r_d \exp\left(c \bullet \ln\left(\frac{f_{y,m}}{f_{y,nom}}\right)\right)$$

The results of these calculations are summarized in Table 8 for the discussed imperfection combinations, (i) leading global and accompanying local and (ii) leading local and accompanying global. The statistical assessment is done using both of the previously mentioned methods, namely, the Δk method and the method developed by Afshan et al.[40], to determine the corrected partial safety factor γ_M^*. The results in Table 8 show the criteria, whether the global or the local imperfection is chosen as a leading imperfection, the applied local imperfection (calibrated, or using the imperfection formula according to Eq.(7)), the applied global imperfection (calibrated or using the formula developed by Somodi et al. Eq.(6) [23]), the mean correction factor b, the number of samples n, the coefficient of variation V_δ, the basic variables CoV V_{rt}^2, the model CoV V_r^2, the corrected partial safety factor γ_M^* and the used method to determine γ_M^*.

It can be seen all values of b are equal to or larger than 1.0, indicating the estimated resistance by the combinations of imperfections are smaller than the target resistance, but by taking the uncertainties into account, it is shown that all the achieved values for the imperfections are larger than 1.0. The partial safety factors obtained using the method developed by Afshan et al.[40] give lower partial safety factors than the Δk method. Asfhan et al.[40] method yielded the smallest corrected partial safety factor $\gamma_M^* = 1.06$ for the combination that comprises the local imperfection as a leading imperfection and the global imperfection as an accompanying imperfection, indicating that this method has the least scatter and discrepancies when compared to the target resistance.

Dividing the samples based on the yield strength:

To test the applicability of each combination on the different types of steel, the full set is divided into smaller sets based on the yield strength (S235, S355, S460). The reliability assessment is performed on the smaller sample sizes. Table 9-Table 11 summarizes the obtained corrected partial safety factor for each steel type. As shown previously, all the mean correction factors b are larger than 1.0, indicating safe results, where the theoretical resistance is smaller than the experimental results. However, the corrected partial safety factors are larger than 1.0. It can be seen that a slight improvement was achieved by dividing the full set into smaller subsets based on the yield strength. As Table 10 shows, the proposed combinations are the safest for S355 with a value of 1.03 for the leading local imperfection and accompanying global imperfection, then comes the leading global imperfection and accompanying local with a value of $\gamma_M^* = 1.06$. For S235 the values of 1.06 and 1.09 for leading local and leading global were achieved, respectively. Finally, for S460, the values of 1.10 and 1.15 for leading local and leading global were achieved, respectively. The obtained combination with the name leading local can be used safely for bridges with corrected partial safety factors less than 1.1.

6. Constant amplitude imperfection factors

According to Annex C of Eurocode EN1993-1-5[4], in combining imperfections, a leading imperfection should be chosen, and the

Table 8
Summary of the parameter uncertainties using the nominal values and overstrength factor.

Criteria	Local imp.	Global imp.	b	n	V_δ	$V_{rt,avg}^2$	$V_{r,avg}^2$	γ^*_M	Method
Leading global	calibrated	Eq. (6) - b curve	1.00	360	0.0511	0.005	0.087	1.19	Δk
Leading local	Eq. (7)	calibrated	1.03	360	0.0480	0.005	0.086	1.13	
Leading global	calibrated	Eq. (6) - b curve	1.00	360	0.0508	0.004	0.007	1.11	Afshan et al. [40]
Leading local	Eq. (7)	calibrated	1.03	360	0.0477	0.004	0.007	1.06	

Table 9
Summary of the parameter uncertainties using the nominal values and overstrength factor for S235.

| Criteria	Local imp.	Global imp.	b	n	V_δ	$V_{rt,avg}^2$	$V_{r,avg}^2$	γ^*_M	Method
Leading global	calibrated	Eq. (6) - b curve	1.00	58	0.0351	0.005	0.079	1.17	Δk
Leading local	Eq. (7)	calibrated	1.04	58	0.0537	0.005	0.089	1.12	
Leading global	calibrated	Eq. (6) - b curve	1.00	58	0.0351	0.010	0.011	1.09	Afshan et al. [40]
Leading local	Eq. (7)	calibrated	1.04	58	0.0537	0.010	0.012	1.06	

Table 10
Summary of the parameter uncertainties using the nominal values and overstrength factor for S355.

Criteria	Local imp.	Global imp.	b	n	V_δ	$V_{rt,avg}^2$	$V_{r,avg}^2$	γ^*_M	Method
Leading global	calibrated	Eq. (6) - b curve	1.01	217	0.0534	0.005	0.089	1.18	Δk
Leading local	Eq. (7)	calibrated	1.02	217	0.0503	0.005	0.087	1.14	
Leading global	calibrated	Eq. (6) - b curve	1.01	217	0.0534	0.008	0.011	1.06	Afshan et al. [40]
Leading local	Eq. (7)	calibrated	1.02	217	0.0503	0.008	0.010	1.03	

Table 11
Summary of the parameter uncertainties using the nominal values and overstrength factor for S460.

| Criteria	Local imp.	Global imp.	b	n	V_δ	$V_{rt,avg}^2$	$V_{r,avg}^2$	γ^*_M	Method
Leading global	calibrated	Eq. (6) - b curve	1.00	84	0.0567	0.005	0.091	1.21	Δk
Leading local	Eq. (7)	calibrated	1.02	84	0.0402	0.005	0.082	1.11	
Leading global	calibrated	Eq. (6) - b curve	1.00	84	0.0567	0.007	0.010	1.15	Afshan et al. [40]
Leading local	Eq. (7)	calibrated	1.02	84	0.0402	0.007	0.009	1.10	
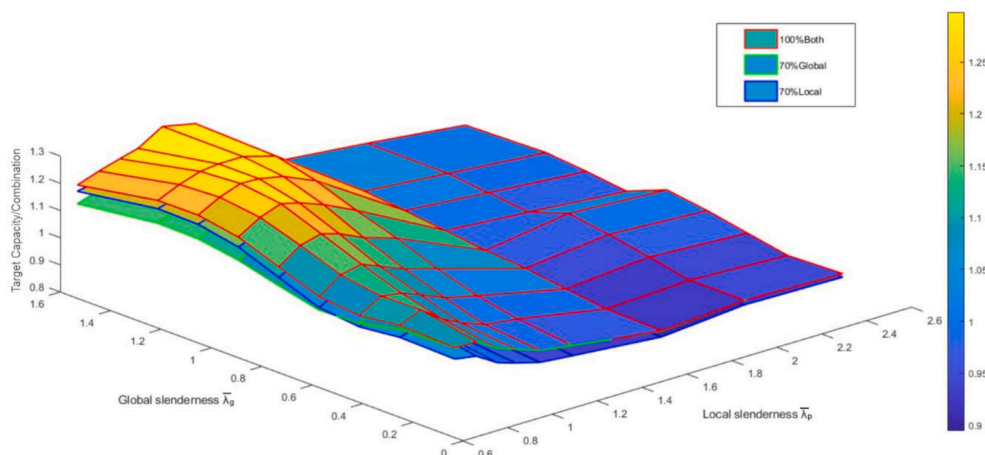
Fig. 12. The ratios of the target capacity to the capacity of each combination, 100 % both (red edges), 70 % global and 100 % local (green edges), 100 %global and 70 %local (blue edges). (For interpretation of the references to colour in this figure legend, the reader is referred to the web version of this article.)

accompanying imperfections may have their values reduced to 70 %. This parametric study tests three different combinations i) both global and local imperfections are applied with their 100 % magnitude. ii) 100 % of the global imperfection is applied, while only 70 % of the local imperfection is applied. iii) 100 % of the local imperfection is applied, while only 70 % of the global imperfection is applied. The parametric study is performed on S235, S355, and S460 on a wide range of global and local slenderness using the previously demonstrated database. As mentioned in the literature review, the authors found that a local imperfection of b/125 would yield the best-fit buckling resistance[6], on average, to the buckling curve developed by Schillo et al.[2] that can be used in FEM-based design. Therefore, this value of imperfection is used here as local imperfection. For global imperfection, the formula developed by Somodi et al.[23] is used to calculate global buckling imperfection, according to Eq.(6). Fig. 12 shows a comparison between the target capacity obtained using the residual stresses to all three studied combinations of imperfections. The x-axis shows the local slenderness ratio $\bar{\lambda}_p$, the y-axis shows the global slenderness ratio $\bar{\lambda}_g$, and the z-axis shows the ratio of the target capacity to the capacity for each combination. Three surfaces are illustrated in the figure where the surface with red edges represents buckling capacity where both local and global imperfections are applied with 100 %, the surface with green edge represents the reduced global combination, and the surface with blue edges represents the reduced local combination. As expected, the 100 % global and local imperfection combination always yields the smallest capacity. For $\bar{\lambda}_g < 0.7$, reducing the global by 70 % yields smaller resistance compared to reducing the local imperfection, then the effect

of reducing the global is less effective as the column is slender.

The same procedures discussed in section 5.3 are used here to statistically evaluate the calculation resistances and to find the corrected partial safety factors for the three different combinations. The target resistance is considered as experimental resistance r_e, and the numerical analysis resistance obtained by using one of the imperfection combinations is considered as the theoretical resistance r_t. The results of the parametric studies are shown in Fig. 13. The figures show comparisons between the buckling resistance obtained using the proposed combinations and the target capacity obtained using the modelling of residual stresses. The top figure is for the combination with 100 % for both global and local. The bottom left figure is for the combination with 70 % reducing local and 100 % global. The last figure is for 100 % local and 70 % global. The blue lines in the figures represent the 5 % and 95 % values. It can be seen that all three combinations yielded results within 5 % of the mean.

Using the equations shown previously, the mean correction factor b, the coefficient of variations V_δ, the basic variables CoV V_{rt}^2, the model CoV V_r^2, and the corrected partial safety factors are determined, as shown in Table 12. All the combinations yield a mean correction factor larger than 1.0, indicating that the obtained average numerical results (r_t) is smaller than the target resistance (r_e). However, the corrected partial safety factors γ^*_M are larger than 1.1 for all the combinations; this happens due to the fact that the scatter is larger for these combinations. This can be demonstrated by taking a look at the value of V_δ and comparing the values to Table 8. The larger value of the coefficient of variation is due to the use of a constant local imperfection factor instead

(a)

(b)

(c)
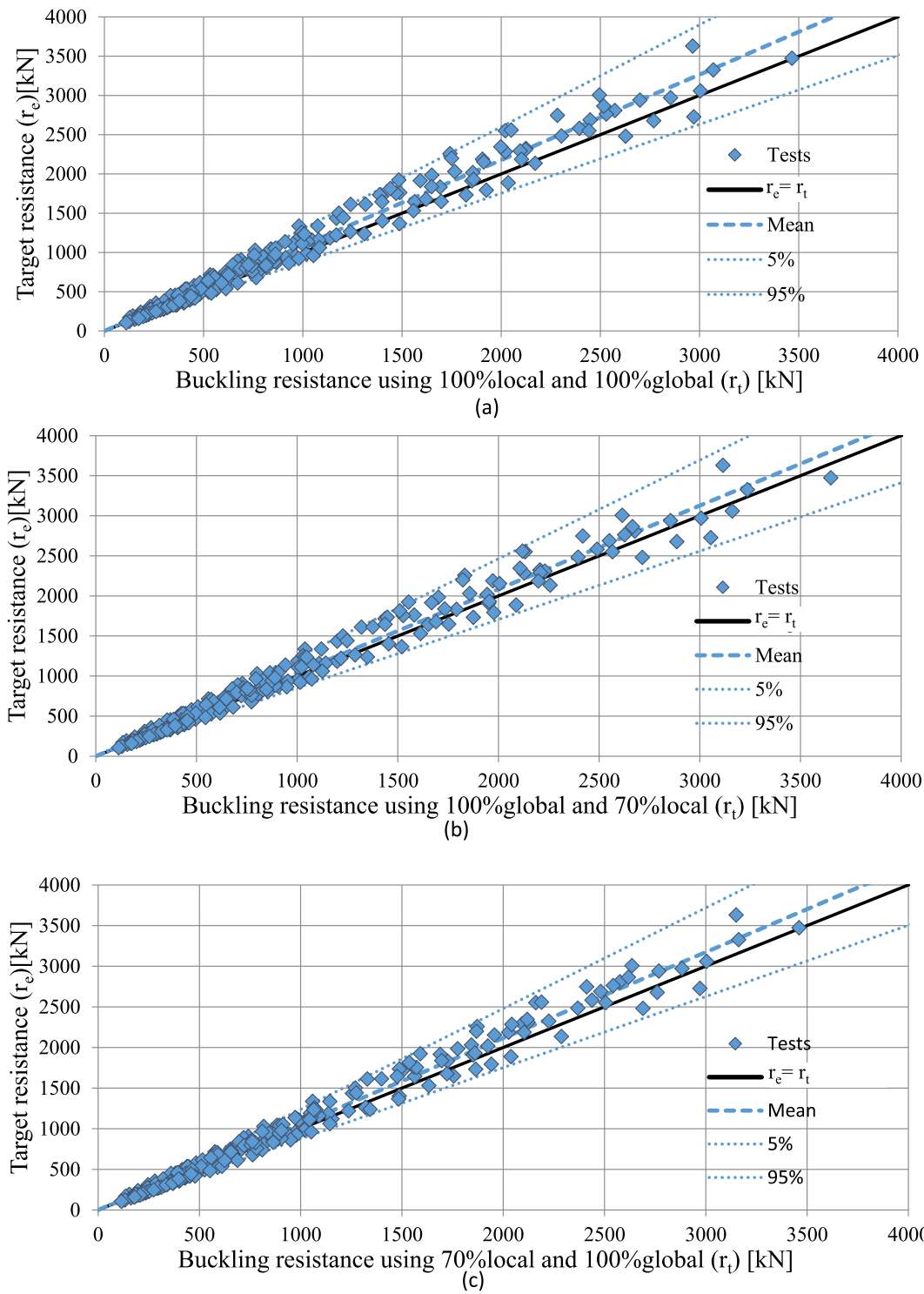
Fig. 13. A comparison between the target resistance r_e (experimental) and the buckling resistance from numerical analyses using a combination of imperfections r_t (theoretical). a) using 100 %global and 100 %local. b) using 100 %global and 70 %local. c) using 70 %global and 100 %local.

Table 12
Summary of the parameter uncertainties using the nominal values and overstrength factor for S235, S355, and S460.

Criteria	Local imp.	Global imp.	b	n	V_δ	$V^2_{rt,avg}$	$V^2_{r,avg}$	γ^*_M	Method
70 % local	0.7*b/125	Eq. (6) - b curve	1.04	237	0.1050	0.005	0.127	1.26	Δk
70 % global	b/125	0.7*b curve	1.06	237	0.0994	0.005	0.122	1.21	
100 % both	b/125	Eq. (6) - b curve	1.09	237	0.1123	0.005	0.133	1.18	
70 % local	0.7*b/125	Eq. (6) - b curve	1.04	237	0.1028	0.004	0.014	1.17	Afshan et al. [40]
70 % global	b/125	0.7*b curve	1.06	237	0.0967	0.004	0.012	1.14	
100 % both	b/125	Eq. (6) - b curve	1.09	237	0.1043	0.004	0.012	1.15	

Table 13
Summary of the parameter uncertainties using the nominal values and overstrength factor for S235.

Criteria	Local imp.	Global imp.	b	n	V_δ	$V_{rt,avg}^2$	$V_{r,avg}^2$	γ^*_M	Method
70 % local	0.7*b/125	b curve formula	1.07	58	0.1189	0.005	0.138	1.25	Δk
70 % global	b/125	0.7*b curve	1.10	58	0.1116	0.005	0.132	1.16	
100 % both	b/125	b curve	1.13	58	0.1281	0.005	0.146	1.15	
70 % local	0.7*b/125	b curve formula	1.07	58	0.1189	0.010	0.024	1.18	Afshan et al. [40]
70 % global	b/125	0.7*b curve	1.10	58	0.1116	0.010	0.022	1.13	
100 % both	b/125	b curve	1.13	58	0.1281	0.010	0.022	1.12	

Table 14
Summary of the parameter uncertainties using the nominal values and overstrength factor for S355.

Criteria	Local imp.	Global imp.	b	n	V_δ	$V_{rt,avg}^2$	$V_{r,avg}^2$	γ^*_M	Method
70 % local	0.7*b/125	b curve formula	1.06	95	0.0968	0.005	0.120	1.20	Δk
70 % global	b/125	0.7*b curve	1.07	95	0.0893	0.005	0.114	1.15	
100 % both	b/125	b curve formula	1.10	95	0.1025	0.005	0.125	1.12	
70 % local	0.7*b/125	b curve formula	1.06	95	0.0968	0.008	0.017	1.11	Afshan et al. [40]
70 % global	b/125	0.7*b curve	1.07	95	0.0893	0.008	0.016	1.08	
100 % both	b/125	b curve formula	1.10	95	0.1025	0.008	0.018	1.07	

Table 15
Summary of the parameter uncertainties using the nominal values and overstrength factor for S460.

Criteria	Local imp.	Global imp.	b	n	V_δ	$V_{rt,avg}^2$	$V_{r,avg}^2$	γ^*_M	Method
70 % local	0.7*b/125	b curve formula	1.02	84	0.0981	0.005	0.121	1.28	Δk
70 % global	b/125	0.7*b curve	1.04	84	0.0938	0.005	0.118	1.23	
100 % both	b/125	b curve	1.07	84	0.1034	0.005	0.125	1.20	
70 % local	0.7*b/125	b curve formula	1.02	84	0.0981	0.007	0.017	1.24	Afshan et al. [40]
70 % global	b/125	0.7*b curve	1.04	84	0.0938	0.007	0.016	1.21	
100 % both	b/125	b curve	1.07	84	0.0938	0.007	0.016	1.18	

of a curve. Therefore, it is always safer to consider the magnitudes of imperfections using special imperfection curves rather than constant values.

Dividing the samples based on the yield strength:

To test the applicability of each combination on the different types of steel, the full set is divided into smaller sets based on the yield strength (S235, S355, S460). The reliability assessment is performed on the smaller sample sizes. Table 13, Table 14 and Table 15 summarizes the obtained corrected partial safety factor for each steel type. As shown previously, all the mean correction factors b are larger than 1.0, indicating safe results, where the theoretical resistance is smaller than the experimental results. However, the corrected partial safety factors are larger than 1.1, except for the combination "reduced global" and the "100 % for both global and local, the obtained γ^*_M are less than 1.1 for S355, indicating that they can be used in bridge design.

7. Conclusions

Different researchers criticised the equivalent imperfection factors available in the Eurocode as they were developed for elastic analysis, and it is inappropriate to use them in GMNI analysis in the FEM design process. Therefore, in this research, two parametric studies were performed to back-calculate equivalent global and local imperfection factors depending on an established database that takes into account the accurate combinations of imperfections and residual stresses that the authors developed in previous research [32]; these combinations showed good agreement to the experimental test results. In this research, accurate best-fits formulas were developed to estimate the appropriate equivalent global and local imperfections factors depending on the global and local slenderness ratios, assuming a leading imperfection and calibrating against the accurate target capacity previously developed. According to Annex D of EN1990[33], a reliability assessment was performed to validate the safety requirements of the developed

equivalent local and global imperfections against the target capacity. Based on the mean correction factor b, it was found that all the proposed combinations of imperfections yield safe results. However, taking the model uncertainties into account, it was found that the proposed equivalent imperfection formulas can be used in FEM-based design with a corrected partial safety factor γ^*_M of 1.06 for S235, 1.03 for S355 and 1.10 for S460.

According to the recommendations of Annex C of Eurocode EN1993-1–5[4], a leading imperfection must be chosen, and the accompanying imperfection value can be reduced to 70 %. Therefore, two additional parametric studies were performed to study this rule using equivalent global and constant local imperfections that represent the local buckling. It was found that for $\bar{\lambda}_g < 0.7$, reducing the global by 70 % yields smaller resistance than reducing the local imperfection; after that range, reducing the local imperfection yields smaller resistances. For S355, these combinations yield a γ^*_M of 1.11 if the local imperfection is reduced by 70 % and a γ^*_M of 1.08 if the global imperfection is reduced. The study showed that it is always safer to use 100 % of both the global and local imperfections, and it leads to an average of 3–4 % resistance decrease compared to the most accurate solution.

For FEM-based design, it is always safe to use both global and local imperfections with 100 % magnitude. The best estimation of the buckling capacity can be achieved by using Eq.(7) as a leading local imperfection and Eq.(14-15) for accompanying global imperfection. For certain ranges of slenderness, one imperfection can be utilised with keeping in mind that the buckling capacity will be overestimated by a certain amount. Applying only the global imperfection using Eq. (6) on the range $\bar{\lambda}_p \leq 0.9 \, and \, \bar{\lambda}_g \geq 0.8$ yields a buckling capacity that is overestimated by less than 5 %.

Declaration of Competing Interest

Acknowledgement

References

[1] European Committee for Standardization (CEN), *EN 1993-1-1 (2005) (English): Eurocode 3: Design of steel structures - Part 1-1: General rules and rules for buildings.* London: British Standards Institute, 2005. [Online]. Available: https://www.phd.eng.br/wp-content/uploads/2015/12/en.1993.1.1.2005.pdf.

[2] Schillo N, Feldmann M, Taras A. Local and Global Buckling of Box Columns Made of High Strength Steel. Universitätsbibliothek der RWTH Aachen; 2017 [Online]. Available:.

[3] H. Degée, A. Detzel, and U. Kuhlmann, "Interaction of global and local buckling in welded RHS compression members," *Int. Colloq. Stab. Ductility Steel Struct. 2006*, vol. 64, no. 7, pp. 755–765, Jul. 2008, 10.1016/j.jcsr.2008.01.032.

[4] European Committee for Standardization (CEN). EN 1993–1-5: 2006 Eurocode 3- Design of steel structures, Part 1. 5: Plated structural elements. London: British Standards Institute; 2006 [Online]. Available:.

[5] Schillo N, Taras A, Feldmann M. Assessing the reliability of local buckling of plates for mild and high strength steels. J Constr Steel Res 2018;142:86–98. https://doi.org/10.1016/j.jcsr.2017.12.001.

[6] Radwan M, Kövesdi B. Local plate buckling type imperfections for NSS and HSS welded box-section columns. Structures Dec. 2021;34:2628–43. https://doi.org/10.1016/j.istruc.2021.09.011.

[7] Clarin M. High strength steel: local buckling and residual stresses. Luleå tekniska universitet 2004.

[8] Schillo N, Feldmann M. Interaction of local and global buckling of box sections made of high strength steel. Thin-Walled Struct 2018;128:126–40. https://doi.org/10.1016/j.tws.2017.07.009.

[9] Khan M, Uy B, Tao Z, Mashiri F. Concentrically loaded slender square hollow and composite columns incorporating high strength properties. Eng Struct 2017;131: 69–89. https://doi.org/10.1016/j.engstruct.2016.10.015.

[10] Yang L, Shi G, Zhao M, Zhou W. Research on interactive buckling behavior of welded steel box-section columns. Thin-Walled Struct 2017;115:34–47. https://doi.org/10.1016/j.tws.2017.01.030.

[11] Usami T, Fukumoto Y. Local and overall buckling of welded box columns. J Struct Div 1982;108(3):525–42. https://doi.org/10.1061/JSDEAG.0005901.

[12] Usami T, Fukumoto Y. Welded box compression members. J Struct Eng 1984;110 (10):2457–70. https://doi.org/10.1061/(ASCE)0733-9445(1984)110:10(2457).

[13] Chern S-P, Lee S-L, Shanmugam NE. Experimental study of thin-walled steel box columns. J Struct Eng 1987;113(10):2208–20. https://doi.org/10.1061/(ASCE)0733-9445(1987)113:10(2208).

[14] Kwon YB, Seo EG. Prediction of the compressive strength of welded RHS columns undergoing buckling interaction. Thin-Walled Struct Jul. 2013;68:141–55. https://doi.org/10.1016/j.tws.2013.03.009.

[15] B. EN, "EN 1090-2: 2008+ A1: 2011 Execution of steel structures and aluminium structures-Technical requirements for steel structures, London," *Br. Stand. Inst. BSI*.

[16] En B. EN 1090–2: 2018 - Execution of steel structures and aluminium structures - Part 2: Technical requirements for steel structures. Br Stand Inst 2018.

[17] Jönsson J, Stan T-C. European column buckling curves and finite element modelling including high strength steels. J Constr Steel Res 2017;128:136–51. https://doi.org/10.1016/j.jcsr.2016.08.013.

[18] J. Rondal and R. Maquoi, *Le flambement des colonnes en acier*. Chambre syndicale des fabricants de tubes d'acier, 1980.

[19] Gonçalves R, Camotim D. On the incorporation of equivalent member imperfections in the in-plane design of steel frames. J Constr Steel Res Sep. 2005;61 (9):1226–40. https://doi.org/10.1016/j.jcsr.2005.01.006.

[20] Lindner J, Kuhlmann U, Just A. Verification of flexural buckling according to Eurocode 3 part 1–1 using bow imperfections. Steel Constr 2016;9(4):349–62. https://doi.org/10.1002/stco.201600004.

[21] Lindner J, Kuhlmann U, Jörg F. Initial bow imperfections e0 for the verification of Flexural Buckling According to Eurocode 3 Part 1 – 1 additional considerations. Steel Constr 2018;11(1):30–41. https://doi.org/10.1002/stco.201700013.

[22] Walport F, Gardner L, Nethercot DA. Equivalent bow imperfections for use in design by second order inelastic analysis. Structures 2020;26:670–85. https://doi.org/10.1016/j.istruc.2020.03.065.

[23] Somodi B, Bärnkopf E, Kövesdi B. Applicable Equivalent Bow Imperfections in GMNIA for Eurocode Buckling Curves – in Case of Box Sections. ce/papers 2022;5 (4):563–7. https://doi.org/10.1002/cepa.1791.

[24] B. Johansson, R. Maquoi, G. Sedlacek, C. Müller, and D. Beg, "Commentary and worked examples to EN 1993-1-5 'Plated structural elements,'" *JRC Sci. Tech. Rep.*, 2007.

[25] "ANSYS® v18." Canonsburg, Pennsylvania, USA, 2021. [Online]. Available: https://www.ansys.com/.

[26] Yun X, Gardner L. Stress-strain curves for hot-rolled steels. J Constr Steel Res 2017; 133:36–46. https://doi.org/10.1016/j.jcsr.2017.01.024.

[27] European Committee for Standardization (CEN), *prEN 1993-1-14:2020: Eurocode 3: Design of steel structures, Part 1-14: Design assisted by Finite element analysis (under development)*. 2021.

[28] Y.-B. Wang, G.-Q. Li, and S.-W. Chen, "The assessment of residual stresses in welded high strength steel box sections," *J. Constr. Steel Res.*, vol. 76, pp. 93–99, 09-01 2012, 10.1016/j.jcsr.2012.03.025.

[29] Khan M, Paradowska A, Uy B, Mashiri F, Tao Z. Residual stresses in high strength steel welded box sections. J Constr Steel Res Jan. 2016;116:55–64. https://doi.org/10.1016/j.jcsr.2015.08.033.

[30] Eccs. European recommendations for steel construction; buckling of steel shells. European Convention for Constructional Steelwork Brussels; 1988.

[31] Schillo N, Feldmann M. Local buckling behaviour of welded box sections made of high-strength steel: Comparing experiments with EC3 and general method. Steel Constr 2015;8(3):179–86.

[32] Radwan M, Kövesdi B. Improved design method for interaction buckling resistance of welded box-section columns. J Constr Steel Res Jul. 2022;194:107334. https://doi.org/10.1016/j.jcsr.2022.107334.

[33] B. European Committee for Standardization (CEN), "Eurocode—Basis of structural design," 2002.

[34] Johansson B, Maquoi R, Sedlacek G. New design rules for plated structures in Eurocode 3. J Constr Steel Res Mar. 2001;57(3):279–311. https://doi.org/10.1016/S0143-974X(00)00020-1.

[35] Vrouwenvelder T. The JCSS probabilistic model code. Struct Saf 1997;19(3): 245–51.

[36] A. Taras and L. S. da Silva, "European Recommendations for the Safety Assessment of Stability Design Rules for Steel Structures," in *Document ECCS–TC8-2012–06–XXX*, 2012.

[37] Simões da Silva L, Tankova T, Marques L, Rebelo C. Comparative Assessment of semi-probablistic methodologies for the safety assessment of stability design rules in the framework of annex D of EN 1990. Coimbra: Univ; 2014.

[38] M. Heinisuo, "Axial resistance of double grade (S355, S420) hollow sections manufactured by SSAB," *Des. Guid. High Strength Struct. Hollow Sect. Manuf. SSAB–for EN 1090 Appl.*, 2014.

[39] Taras A, Huemer S. On the influence of the load sequence on the structural reliability of steel members and frames. Structures 2015;4:91–104.

[40] Afshan S, Francis P, Baddoo NR, Gardner L. Reliability analysis of structural stainless steel design provisions. J Constr Steel Res Nov. 2015;114:293–304. https://doi.org/10.1016/j.jcsr.2015.08.012.

[41] Tuezney S, Lauwens K, Afshan S, Rossi B. Buckling of stainless steel welded I-section columns. Eng Struct Jun. 2021;236:111815. https://doi.org/10.1016/j.engstruct.2020.111815.

[42] Radwan M, Kövesdi B. Equivalent local imperfections for FEM-based design of welded box sections. J. Constr. Steel Res. 2022;199:107636. https://doi.org/10.1016/j.jcsr.2022.107636.